Measurement of the Void Fraction of Gas-Liquid Two-Phase CO_2 Flow Using Laser Attenuation Techniques

Quansheng Duan[a], Ju Peng[a], Lijuan Wang[b], Yong Yan[b*]

[a] School of Control and Computer Engineering
North China Electric Power University, Beijing 102206, China
[b] School of Engineering and Digital Arts
University of Kent, Canterbury, Kent CT2 7NT, U.K.

***Abstract*—Carbon capture and storage (CCS) is a promising technology to reduce CO_2 emissions from industrial processes. However, void fraction measurement is one of the challenging issues to be solved for gas-liquid two-phase CO_2 flow measurement. This paper presents a novel measurement system using laser intensity attenuation techniques to measure the void fraction of two-phase CO_2 flow. The measurement system includes optical sensors, a laser detector array and a monolithic processor. The performance of the proposed measurement system is verified through experimental tests under various conditions, including stratified flow and bubbly flow. The void fraction of two-phase CO_2 flow ranges from 0 to 69%. Experimental results demonstrate that the system is capable of measuring the void fraction of CO_2 flow with an error between -2% and 3.6%.**

Keywords—CCS, gas-liquid two-phase CO_2 flow, void fraction, optical sensors, laser intensity attenuation

I. aINTRODUCTION

Carbon Capture and Storage (CCS) is a promising technology with great significance to many industrial fields and scientific research [1, 2]. The ecological balance of the earth is directly affected by carbon dioxide (CO_2) as it is an important meteorological parameter in the atmosphere. During long-distance pipeline transportation from capture to storage sites, pipeline pressure and temperature are variable according to the local climate, which may lead to phase change of CO_2 [3]. In order to measure the total mass flow rate of CO_2 accurately, it is necessary to quantify the void fraction of gas-liquid two-phase CO_2 flow.

Laser sensors have been widely used in variety of sensing and detection areas in recent years with advantages of high sensitivity, rapid response and good durability [4]. Optical sensors offer nonintrusive and noninvasive measurements which would not influence the flow state during the measurement process. In comparison with other common techniques such as Electrical Capacitance Tomography (ECT) and differential-pressure based methods, the laser attenuation based system is little affected by the inputs and outputs of the system and hence produces more accurate measurements with high sensitivity. In addition, the system can be easily calibrated under static conditions to achieve high accuracy and reliability. Optical sensors offer nonintrusive and nondestructive measurements which would not influence the flow state during the measurement process. Recently, laser spectroscopy has been applied to fluid measurement with the advantages of fast response, high sensitivity and low maintenance [12].

Optical sensing and detection is considered as an effective method for two-phase flow measurement. For instance, medium-infrared difference frequency detection technology, integral cavity output spectroscopy technology, laser-radar technology and tunable diode laser absorption spectroscopy have been proposed for the measurement of air-water two-phase flow [7, 8, 13]. However, there are limited research on the measurement of the void fraction of two-phase CO_2 flow. This study aims to develop a novel measurement system using laser attenuation techniques to measure the void fraction of two-phase CO_2 flow under CCS conditions. The measurement principle and experimental validation of the system are presented.

II. METHODOLOGY

A. Laser Attenuation Detection

Laser intensity attenuation is a predominant method for gas-liquid two-phase flow measurement due to its simple principle [11, 12]. A laser source is placed on one side of the observation window and a detector on the other side to detect the optical intensity. The void fraction of CO_2 in the pipeline can be calculated according to the intensity of incident beam and outgoing beam [6].

Laser attenuation detection is based on the classic Lambert-Beer law, which is represented by the following equation [10]:

$$I = I_0^{-\varepsilon d\beta} \quad (1)$$

$$T = \frac{I}{I_0} \quad (2)$$

Where I_0 and I are the intensities of the incident and transmitted laser beam, respectively. ε is the molar absorption coefficient. β is the concentration of the medium and d is the path length of the laser beam in the fluid.

The transmission of the laser beam (T) is defined as the ratio of I_0 and I.

B. Sensor Design

As shown in Fig. 1, a total of twelve sensors are used to constitute a sensor array. The observation window is made of polymethyl methacrylate (PMMA) due to its high transmittance of laser beams. In order to reduce the absorption and reflection of laser beams by the pipeline, the inner surface of the pipeline is coated with dark paint. The inner diameter of the pipeline is 25 mm, and the outer diameter of the observation window is 100 mm. The maximum withstand pressure is 8 MPa whilst the range of withstand temperature is 5-50℃.

Radial optical components are adopted in the laser detector array to obtain the attenuation rate of each laser beam by the two-phase flow in the pipeline. The attenuation of laser optical intensity is proportional to the amount of gaseous CO_2 in the pipeline. The higher the void fraction, the weaker the transmitted signal. The optical sensing system would be affected by external optical sources or internal optical reflections. For this reason, an optical encloser is used to ensure the sensing unit is light-tight.

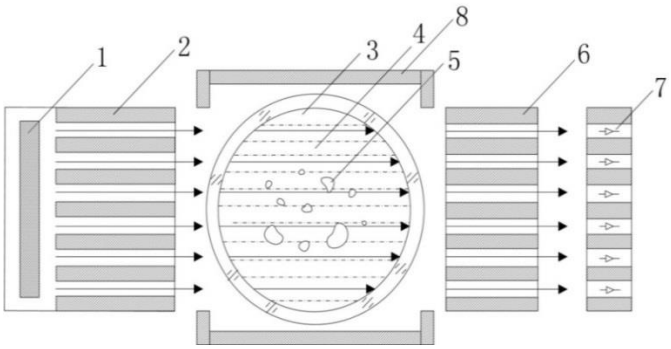

1- Linear laser source with prism
2–Linear laser source collimator
3–Sensor pipe section
4- CO_2 two-phase flow
5- Bubble
6- Detector collimator
7- Laser detector array (double row)
8- Optical Encloser

Fig. 1. Cross-sectional view of the sensing arrangement

As shown in Fig. 2, two linear laser sources are arranged in parallel within the encloser. A prism is used to convert the laser source from a point source to a linear source and minimize the attenuation of the laser intensity. The cross section of each collimator is square shaped. A collimated laser beam is produced by passing through the prism and the collimator in sequence. The two sets of parallel laser beams are staggered to avoid the interference caused by different flow patterns.

For each laser beam, the following relationship is valid if all the parallel beams are well collimated and monochromatic [15]

$$\alpha_M = -\frac{1}{N(I_l - I_g)} \sum_{n=1}^{N} I_n + \frac{I_l}{I_l - I_g} \quad (3)$$

where α_M is the measured void fraction, N is the total number of laser beams in the sensor array, I_g and I_l are the optical intensities in the pure gas phase and pure liquid phase, respectively.

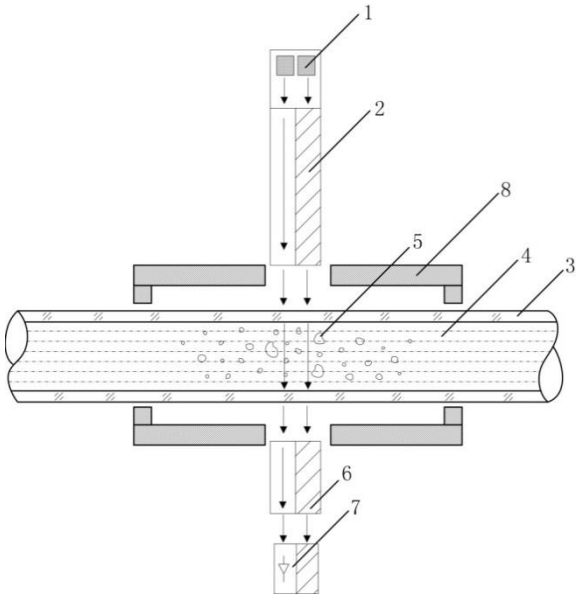

1- Linear laser source with prism
2–Linear laser source collimator
3–Sensor pipe section
4- CO_2 two-phase flow
5- Bubbles
6- Detector collimator
7- Laser detector array (double row)
8- Optical Encloser

Fig. 2. The plan view of the sensor arrangement

The parallel laser beams are partly absorbed after passing the fluid to be measured. The source collimator is placed coaxially with the detector collimator to make sure the irradiated line is straight. Discrete interrogation of the pipeline is ensured by completing collimation of the laser beams, so the scattering can be effectively reduced. As shown in Fig. 3, each laser beam element has a width W of 8 mm and a uniform spacing G of 5 mm. The 'dead space' between the laser beams is avoided within the axial length of 2W+G, so that no part of the pipe cross-section is left uninterrogated by the laser beams [5].

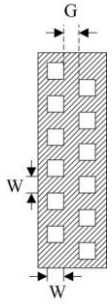

Fig. 3. Layout of the collimator

The wavelength of the laser source is 694.3 nm, which

is the peak of infrared absorption of CO_2. The power of laser is 100 mW. In order to drive the laser source, a timer is employed to generate pulse signals with adjustable duty cycles. Two coolers, i.e. thermoelectric cooler (TEC) and optical source internal integrated semiconductor cooler are used to achieve the system temperature control as the laser detection system is sensitive to temperature. In order to improve the stability of the sensor, a temperature control circuit is used to maintain the temperature of the system within a constant range.

C. Signal Conditioning and Processing

Photocurrent is produced by the photoelectric detector without the input of an optical signal, which is known as the dark current. It is the combined action of the parasitic resistance and the bias voltage of the detector, and the non-bias structure is used to avoid this phenomenon.

The signal of optical intensity is converted into a weak photocurrent signal by the detector, and the amplification for the weak signal is realized through lock-in amplification. The pre-amplified photocurrent is magnified with a reference signal together by a lock-in amplifier, and the frequency of the signal is equal to the drive signal. The DC component corresponding to the cross-sectional void fraction is obtained.

The signal obtained by the photosensitive sensor is transmitted to a STM32 monolithic processor before being sent to the host computer via serial bus [14].

III. EXPERIMENTAL RESULTS AND DISCUSSION

A. Test Faculity and Test Conditions

Fig. 4 shows the schematic diagram of gas-liquid two-phase CO_2 flow test rig. A circulator and air compressor supply powers for gaseous and liquid CO_2 fluids in the pipeline, respectively. Two-phase CO_2 flow is fully mixed in the mixer, goes through the red pipe (see Fig.4) and then return to the separator. The two sets of laser generators and optical intensity detection devices are mounted on the horizontal and vertical test sections, respectively.

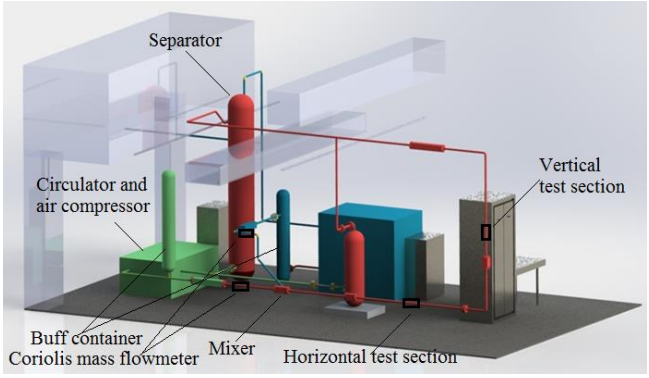

Fig. 4. Schematic diagram of gas-liquid two-phase CO_2 flow test rig

Buffer containers are mounted in the single phase flow pipelines to reduce the pulsation of the fluid and ensure stable and continuous flow during experiments. Coriolis mass flowmeters are fixed on single liquid and single gas CO_2 flow sections, respectively, to provide mass flowrate, density and temperature of the single phase flows [9]. The range of the fluid temperature is 20~30℃, whilst the test pressure is between 5.7 MPa and 7.2 MPa. The void fraction during the experimental tests in this research ranges from 0 to 69%. The maximum void fraction (69%) is determined by the operating conditions of the test rig. Once the void fraction exceeds 69%~70%, CO_2 in the single-phase gas section will be liquidized due to high differential-pressure between the inlet and outlet of the air compressor. For this season, the maximum void fraction is set to 69% to ensure pure gas CO_2 in the single-phase gas section.

As the void fraction is approximate to gas volume fraction when the slip effect between the two phases is ignored, gas volume fraction α is used in this study as reference and calculated according to the outputs of Coriolis mass flowmeters:

$$\alpha_r = \frac{q_g}{q_g+q_l} \tag{4}$$

where α_r is the gas volume fraction, q_l and q_g are the volumetric flowrates of liquid and gaseous CO_2 flows.

B. Results and Discussion

In order to obtain the initial optical intensity, the experimental tests were firstly conducted with vacuum pipelines. Optical intensity was acquired and recorded for 5 min with a sampling frequency of 50 Hz. The averaged intensity is defined as the initial optical intensity I_α. Thereafter, experimental tests were undertaken with single gas and single liquid CO_2 flows, respectively. The difference between the measured optical intensity and the initial optical intensity is I_g or I_l.

To verify the proposed measurement method, stratified flow and bubbly flow with different gas void fractions were tested, respectively. The void fraction α_M is obtained through measuring the optical intensity and calculated with equation (3). The reference void fraction α_r is calculated from equation (4) according to the outputs of Coriolis mass flowmeters.

During the experiments, the optical intensity ranges from 4.421 lx to 1919.887 lx with a standard deviation between 0.281 and 32.243. The average temperature is 21.15 ℃ and pressure in the pipe is 5.73 MPa. Fig. 5 shows the measurement errors on the horizontal test section for different flow patterns. Fig. 5 (a) and (b) plot the absolute errors in stratified flow with various void fraction ranges. When the void fraction is less 8%, the deviation of α_M from the reference is within ±0.4%. Once the gas entrainment is increased, the measurement error keeps in the same level. Fig. 5 (c) and (d) depict the errors of measured void fraction in bubbly flow. It is obvious that the errors are larger than those in stratified flow, with the range of ±1.5%. Some factors, such as the influence of slip ratio, the size of the bubble and the distribution of flowrate affect the measurement of void fraction. However, using a collimating sensor array helps to reduce the influence of different flow

patterns

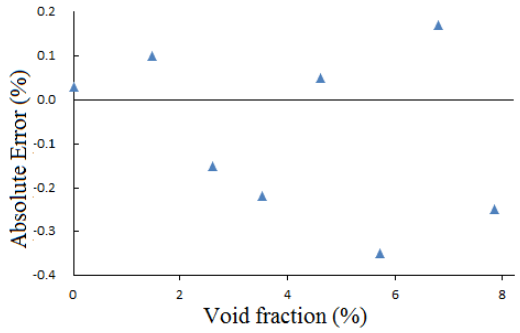

(temperature: 21.13℃, pressure: 5.51 MPa, flow rate: 1.73m/s)

(a) Stratified flow with void fraction from 0% to 8%

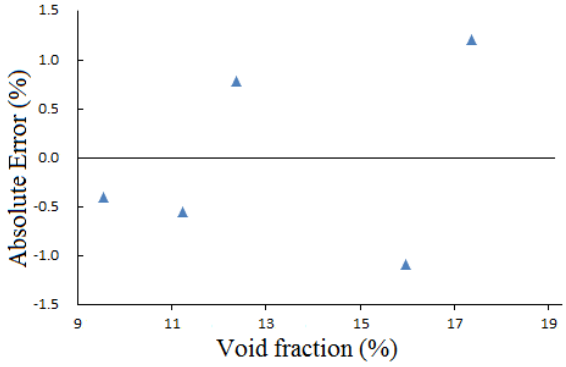

(temperature: 21.15℃, pressure: 5.83 MPa, flow rate: 0.29m/s)

(b) Stratified flow with void fraction from 40% to 70%

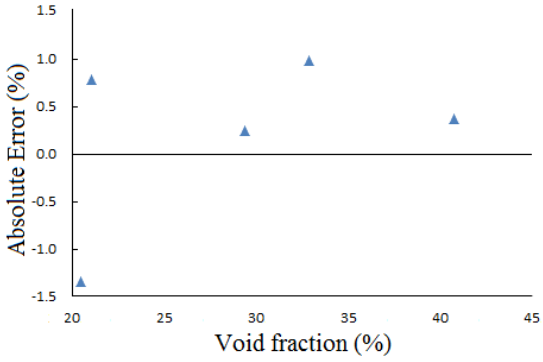

(temperature: 21.14℃, pressure: 5.78MPa, flow rate: 1.72m/s)

(c) Bubbly flow with void fraction from 9% to 20%

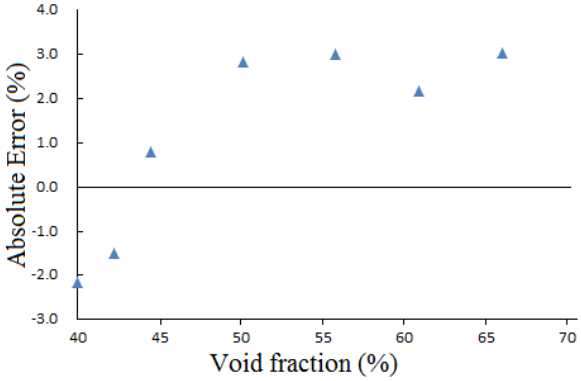

(temperature: 21.16℃, pressure: 5.80 MPa, flow rate: 0.86m/s)

(d) Bubbly flow with void fraction from 20% to 45%

Fig. 5. Measurement errors of void fraction in horizontal section

Fig. (6) shows the measurement errors on vertical test section in bubbly flow. The void fraction ranges from 0 to 45%. Fig. 6 (a)-(d) show that the errors increase with the amount of entrained gas. Through comparing the results of bubbly flow in vertical section (Fig. 6 (a)-(d)) and horizontal section (Fig. 5 (c) and (d)), the measurement errors in horizontal section are smaller than those in horizontal section under the same void fraction. This is due to the fact that the bubbles in a vertical pipe are more evenly distributed than those in a horizontal pipe due to gravity and buoyancy.

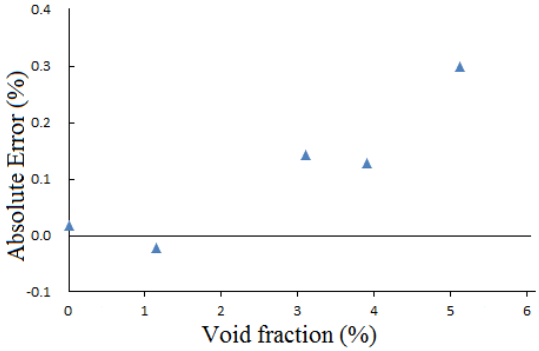

(temperature: 22.69℃, pressure: 5.81 MPa, flow rate: 1.73m/s)

(a) Bubbly flow with void fraction from 0% to 5%

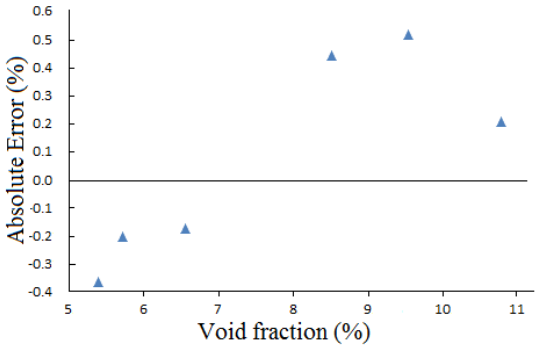

(temperature: 22.67℃, pressure: 5.82 MPa, flow rate: 1.67m/s)

(b) Bubbly flow with void fraction from 5% to 11%

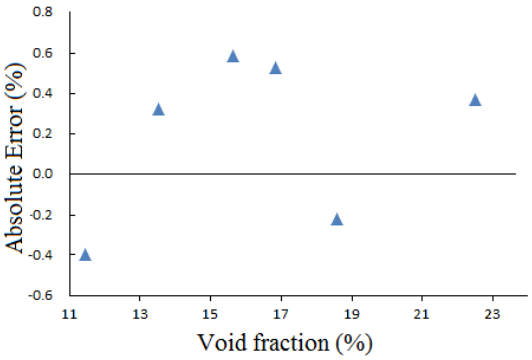

(temperature: 21.76℃, pressure: 5.81 MPa, flow rate: 1.65m/s)

(c) Bubbly flow with void fraction from 11% to 23%

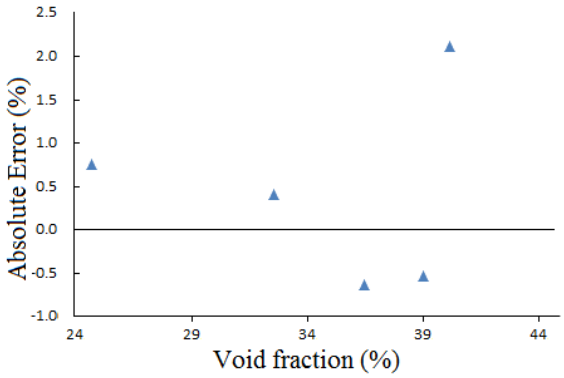

(temperature: 21.65℃, pressure: 5.81 MPa, flow rate: 0.27m/s)

(d) Bubbly flow with void fraction from 24% to 45%

Fig. 6. Measurement errors of void fraction in vertical section

IV. Conclusions

A simple and effective method using on-line laser detection techniques to measure the void fraction of CO_2 gas-liquid two-phase flow has been proposed through theoretical analysis and experimental verification. The experiments were conducted with the void fraction ranging from 1% to 69% for different flow rates and flow patterns. The results have been compared with reference data calculated according to the outputs from the Coriolis mass flowmeters. It has been found that the measured void fraction agrees well with the reference values with a maximum absolute error of 3.57%. The results presented have indicated that the proposed measurement system is capable of achieving non-contact, accurate and reliable measurement of the void fraction of two-phase CO_2 flow under CCS conditions.

Acknowledgments

The authors would like to acknowledge the financial support of the UK CCS Research Centre (www.ukccsrc.ac.uk) in carrying out this work. The UK CCSRC is funded by the EPSRC as part of the RCUK Energy Programme. This work is also supported in part by the 111 Talent Introduction Projects (B13009) at North China Electric Power University

References

[1] W. Cai, and D. I. Singham, “A principal-agent problem with heterogeneous demand distributions for a carbon capture and storage system,” Eur. J. Oper. Res. vol. 264, pp. 239-256, January 2018.

[2] S. W. Jin, Y. P. Li and S. Nie, “The potential role of carbon capture and storage technology in sustainable electric-power systems under multiple uncertainties,” Renew. Sust. Energ. Rev. vol. 80, pp. 467-480, December. 2017.

[3] Y. J. Kim, W. He and D. Ko, “Increased N_2O emission by inhibited plant growth in the CO_2 leaked soil environment: Simulation of CO_2 leakage from carbon capture and storage (CCS) site,” Sci. Total Environ. vol. 607, pp. 1278-1285, December 2017.

[4] S. Rai, V. Madan and J. P. August, “Favre-Racouchot syndrome: a novel two-step treatment approach using the carbon dioxide laser,” Brit J Dermatol, vol. 107, pp. 657-660, March. 2014.

[5] I. R. Barratt, Y. Yan and B. Byrne, “Mass flow measurement of pneumatically conveyed solids using radiometric sensors”, Flow Meas. Instrum., vol. 3, pp. 223-235, November. 2000.

[6] A. Suzuki and K. Ohta, “Mechanical properties of poly(ethylene terephthalate) nanofiber three-dimensional structure prepared by CO_2 laser supersonic drawing,” J. Appl. Polym. Sci. vol. 135, January 2018.

[7] A. M. Hegab, S. A. Gutub and A.Balabel, “A Developed Numerical Method for Turbulent Unsteady Fluid Flow in Two-Phase Systems with Moving Interface,” Int. J. Comput. Methods. vol. 14, December. 2017.

[8] M. Chai, K. Luo and C. Shao, “An efficient level set remedy approach for simulations of two-phase flow based on sigmoid function,” Chem. Eng. Sci. vol. 172, pp. 335-352, November 2017.

[9] M. J. Ahammad, J. M. Alam and M. A. Rahman, “Numerical simulation of two-phase flow in porous media using a wavelet based phase-field method,” Chem. Eng. Sci. vol. 173, pp. 230-241, December 2017.

[10] V. M osorov, “The Lambert-Beer law in time domain form and its application,” Appl. Radiat. Isot. vol. 128, pp. 1-5, October. 2017.

[11] K. Uckert, A. Grubisic and X. Li, “IR resonance-enhanced organic detection with two-step laser desorption time-of-foptical mass spectrometry,” ICARUS, vol. 299, pp. 15-21, January. 2018.

[12] E. Sherif, F. Ashraf and H. S. Ayoub, “The design and implementation of photoacoustic based laser warning receiver for harsh environments,” Opt Laser Technol. vol. 98, pp. 385-396, January 2018..

[13] M. A. Tabrizi, M. Shamsipur, and R. Saber, “A high sensitive visible optical-driven photoelectrochemical aptasensor for shrimp allergen tropomyosin detection using graphitic carbon nitride-TiO_2 nanocomposite,” Biosens Bioelectron, vol. 98, pp. 113-118, December 2017

[14] F. Yang, C. Ma and H. Li, “Design of Wireless Video Transmission System based on STM32 Microcontroller,” AMME, vol. 1820, Wuhan, 25-26 February 2017

[15] R. Liu, X. Chen and M. Yao, “Development of an automatic measuring device for total sugar content in chlortetracycline fermenter based on STM32,” ICEIE, Nanjing, vol. 10322, 17-18 September 2016.